Journal Pre-proofs

Regular Article

Nanoscale Insight into the Relation between Pressure Solution of Calcite and Interfacial Friction

Binxin Fu, Yijue Diao, Rosa M. Espinosa-Marzal

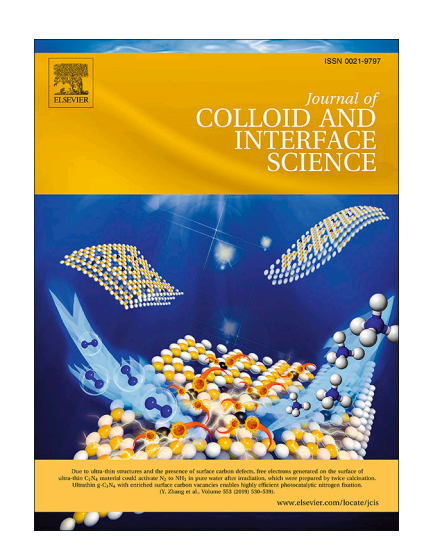
PII: S0021-9797(21)00676-7

DOI: https://doi.org/10.1016/j.jcis.2021.04.145

Reference: YJCIS 28012

To appear in: Journal of Colloid and Interface Science

Received Date: 24 February 2021 Revised Date: 29 March 2021 Accepted Date: 30 April 2021



Please cite this article as: B. Fu, Y. Diao, R.M. Espinosa-Marzal, Nanoscale Insight into the Relation between Pressure Solution of Calcite and Interfacial Friction, *Journal of Colloid and Interface Science* (2021), doi: https://doi.org/10.1016/j.jcis.2021.04.145

This is a PDF file of an article that has undergone enhancements after acceptance, such as the addition of a cover page and metadata, and formatting for readability, but it is not yet the definitive version of record. This version will undergo additional copyediting, typesetting and review before it is published in its final form, but we are providing this version to give early visibility of the article. Please note that, during the production process, errors may be discovered which could affect the content, and all legal disclaimers that apply to the journal pertain.

© 2021 Elsevier Inc. All rights reserved.

Nanoscale Insight into the Relation between Pressure Solution of Calcite and Interfacial Friction

Binxin Fu¹, Yijue Diao¹, and Rosa M. Espinosa-Marzal^{1,2*}

1 Department of Civil and Environmental Engineering, University of Illinois at Urbana-Champaign, 205

N. Matthews Avenue, Urbana, IL 61801, United States.

2 Department of Materials Science and Engineering, University of Illinois at Urbana-Champaign, 1304

W. Green St., Urbana, IL 61801, United States

*Corresponding author

Rosa M. Espinosa-Marzal, Tel: +1 217 607 3856, Email: rosae@illinois.edu

Keywords: pressure solution, friction, calcite, Surface Forces Apparatus, Atomic Force Microscope

Abstract

Pressure solution of carbonate-based rocks participates in many geophysical and geochemical processes, but fundamental knowledge of the interfacial processes is still lacking. By concurrently pressing and sliding two single calcite crystals past each other, the pressure solution rate and the friction force between the crystals were concurrently measured in calcium-carbonate saturated water with an extended surface forces apparatus. These studies reveal that both a decrease and an increase in frictional strength can originate from the pressure-solution of calcite single crystals. By conducting nanoscale force measurements with an atomic force microscope, ion specific effects were unveiled at the level of a single asperity. Pressure solution is promoted when the interfacial water layers of calcite remain undisturbed under stress (e.g. with Ca(II)) and the dissolved ions and water lubricate the interface – a phenomenon called pressure-solution facilitated slip. The mechanically induced disruption of the hydration layers of the calcite surface (e.g. with Mg(II) and low Ni(II) concentration) correlates with the more fluid-like and lubricious behavior of the confined fluid in the absence of pressure solution. Charge neutralization of the calcite surface leads to an abrupt change of calcite's hydration layers, which promotes pressure-solution facilitated slip. This work advances the fundamental understanding of physicochemical interactions occurring at confined surfaces of stressed calcite.

1. Introduction

Pressure solution of minerals at grain boundaries is the major mechanism of ductile deformation of the Earth's upper crust [1], and plays a critical role in a variety of geological processes, such as diagenesis [2] and inter-seismic fault healing [3]. Pressure solution happens because the contact stress on mineral grains enhances the chemical potential of the stressed solid and thereby its solubility above that of the stress-free mineral. The local increase in solubility leads to a dramatic undersaturation of the interfacial fluid and thereby to mineral dissolution [4]. The fluid film confined at the grain boundaries serves as a diffusion path for the transport of the dissolved mineral toward less stressed regions nearby, where the mineral reprecipitates. Carbonate-based rocks abound in the lithosphere and a number of studies have focused on the pressure solution of calcite, which is the most stable crystalline polymorph of calcium carbonate [1]. These studies have been largely focused on compaction of granular systems [5-7] and on indentation measurements on single crystals [8, 9]. The effects of grain size, effective stress and fluid chemistry [10-12] on crystal deformation have been investigated, but the complexity of the granular system and the high indentation stress make it challenging to unambiguously deconvolute pressure solution from other deformation mechanisms, including plastic deformation [5], grain boundary sliding [13] or crack formation [9]. This limitation motivated the extension of our Surface Forces Apparatus (SFA) to measurements on pairs of calcite single crystals [14]. This highly mechanically and thermally stable technique measures the deformation rate of two single calcite crystals undergoing pressure solution with ~1 nm measuring precision of the crystal thickness. The nanoscale studies revealed how the pressure solution is influenced by the molecular composition of the calcite/fluid interface and is sensitive to the ion concentration[14].

Calcite acquires a small negative charge upon exposure to water[15], as inferred from zeta potential measurements of calcite microparticles[16]. The near-surface concentration of co-ions, the ions with the same charge sign as the surface (CO_3^{-2} and HCO_3^{-1}), is thus expected to be smaller than that of the counter-ions. The "hydration-driven" interaction of calcite with counterions relies on the strong hydrophilicity of calcite, which leads to the adsorption of two highly ordered water "ice-like" layers [17]. The term ice-like implies the pronounced order of the water molecules bound to the calcite's surface and the prominent slowdown of the diffusivity of these molecules. Calculations of the free energy of adsorption by Kerisit and Parker [17] indicated that the outersphere calcium ions (OS-Ca²⁺ at ~4.9 Å from the unconfined calcite surface) are favored compared to the inner-sphere calcium (IS-Ca²⁺) ions (at ~3.3 Å from the calcite surface)[17]. Their calculations also suggested that cations forming a strong bond with water can disrupt the hydration layers of the surface and thus retain a full coordination shell once adsorbed as IS complexes on the surface. For example, magnesium was predicted to form a more stable IS complex than calcium due to its strong interaction with the solvent and the surface. Ricci et al.[18] also concluded that Ca²⁺ was present in the vicinity of the calcite surface, but weakly bound, and the tip was able to push the cations away while scanning the surface. Their simulations also suggested that the energy penalty to penetrate the "ice-like water layers of calcite prevented strongly hydrated ions from directly adsorbing onto the surface. Later calculations by Raiteri et al. [19] did not found IS complexes for Ca²⁺ and concluded that calcium does not adsorb on the basal plane of calcite. In agreement with this, recent computational studies and experiments have shown the lack of an attractive potential energy well in the interaction between divalent ions and the calcite surface at equilibrium, which explains the low coverage of the basal plane of the unconfined calcite surfaces with counterions [15, 19, 20].

Deviations from this behavior have been reported for the "confined" calcite-solution interface, which is of relevance during pressure solution [16]. For example, the studies by Ricci et al. investigated adsorption of Rb⁺ on the calcite surface by Atomic Force Microscopy (AFM) imaging. The adsorbed Rb⁺ appeared to adsorb every other oxygen row along the [010] direction and the tip had to apply a higher load to remove it [18]. This suggests a higher surface coverage compared to the X-ray reflectivity measurements on unconfined calcite [15]. We demonstrated the enrichment of ions at the vicinity of the confined calcite surface as well as ion specific effects using AFM force spectroscopy. We reported that strongly hydrated Ca²⁺ ions stay on top of calcite's hydration layers even under normal stress [16]. In contrast, Na⁺, a less strongly hydrated metal cation, can lose part of its hydration shell and penetrate through the hydration layers of the confined calcite surface [21]. This leads to the distortion of the hydration layers and to slower pressure-induced dissolution of calcite [14]. No other ion specific effects have been reported yet.

Emerging evidence suggests that the fault strength (friction) can be weakened in the presence of reactive brines due to the dissolution and/or chemical alteration of the minerals that interact with the fluid [22-24]. In laboratory experiments on water-saturated calcite-rich gouge, pressure solution was observed concurrent with a reduction in friction compared to dry conditions [5]. In contrast, reprecipitation of calcite after its pressure-induced dissolution was related to contact healing and overall gouge compaction [25] and to an increase in the friction coefficient [6]. The seemingly contradictory observations likely arise from the complexity of the investigated systems and the concurrent action of multiple mechanisms. This motivated our friction force measurements on nanosized single asperity contacts between a calcite single crystal and an oxidized silicon AFM tip. These studies revealed three pathways of energy dissipation in aqueous environment [21, 26]: viscous shear of a lubricious solution film at low normal stresses, like an oil film that lubricates the gear in a motor; shear-promoted thermally-activated slip at intermediate normal stresses, similar to dry friction but strongly influenced by the hydrated ions localized at the interface; and a prominent decrease in friction with increasing load at sufficiently slow sliding velocities and highest investigated normal stresses, called pressure-solution facilitated slip. It was hypothesized that frictional weakening could result from the pressure solution of calcite and promote fault slips and Earthquake nucleation, e.g., upon fluid injection.

The present work provides the first direct evidence for the relation between pressure solution of calcite single crystals and their frictional characteristics. We are able to compare results at the nanoscale (on single asperity contact, by AFM) and at contacts of ~1000 µm² (representing "macroscale" contacts between calcite surfaces, by SFA) for the first time. We confirm that the phenomenon of pressure-solution facilitated slip also happens at macroscale contacts and provide additional evidence for the increase in friction due to the concurrent precipitation within the contact. Furthermore, this work expands the types of ion specific effects on the friction force through the study of three divalent cations, Ca²+, Ni²+, and Mg²+ at the level of a single asperity. The range of concentrations simulates Ca²+ concentrations in nature, from ground water [27] to concentrated brines [28]. Ni²+ is a common contaminant from industrial and mining activity, and hence, present in injected fluids, with great toxicity and some isotopes like ⁵⁶Ni and ⁵⁷Ni exhibiting radioactivity; and it also interacts strongly with calcite and can be incorporated into the crystal lattice [29]. Mg²+ is a major divalent cation in seawater that also incorporates into carbonate rocks [30]. Ion-specific effects on calcite's frictional behavior and pressure solution, although originated at the molecular level, are expected to influence the strength of mineral interfaces at geological scales.

2. Methods and materials

Calcium carbonate (purity ≥ 99.0%, Sigma-Aldrich) was added in excess to DI water to achieve saturation of the solution at room temperature for at least 24 hours. Nickel chloride hexahydrate, magnesium chloride and calcium chloride (purity of three salts $\geq 99.0\%$, Sigma-Aldrich) were dissolved in solutions equilibrated with excess calcium carbonate (CaCO₃) solid, with a concentration of 0 (no salt added), 0.1, 1, 10 and 100 mM and equilibrated for at least 1 day. Iceland Spar calcite single crystals were employed for SFA and AFM experiments with the cleaved calcite plane ($10\overline{1}4$) facing the solution (Figure S2). The cleaved calcite samples were first immersed and equilibrated with calcium carbonate saturated solution for 24 h prior to the measurements (0.515 mM CaCO₃ at 25 °C). All solutions were filtered with 0.22 µm PTFE hydrophilic syringe filters (Thermo Fisher Scientific) before use. Our SFA[31] was extended to carry out interferometric measurements of the crystal thickness [14] with concurrent friction-force measurements. An AFM (Nanowizard, JPK Instruments) located in an acoustic chamber was used for surface force and friction force measurements on single calcite crystals using oxidized silicon tips and silica microspheres (Figure S3-S4). The cell was covered with a membrane to prevent evaporation during the experiment, and it was rinsed three times with new solution and reequilibrated for 1h every time the solution concentration was changed. The pH was measured before the begin of the AFM experiment and compared to the expected value in equilibrium (Table S1). More details about the experimental methods can be found in the SI Text.

3. Results

3.1 Surface Forces Apparatus (SFA) measurements of crystal thickness and friction force

A SFA was modified to perform interferometric measurements with two single calcite crystals pressing each other at constant load L and immersed in an aqueous solution of known composition [14]. The method provides the change in crystal thickness (ΔT) in real time with a precision of ± 1 nm while the crystal dissolves and grows; see details in the SI Text and the schematics in Figure 1A. Here, we perform interferometric coupled with friction-force measurements between two calcite single crystals in equilibrium with water (0.515 mM CaCO₃, pH 8.35). The bottom crystal is fixed to a spring that can be moved upwards and downwards by a (normal) piezo and deflect only in the normal direction, while the upper crystal is mounted on a spring that can be moved sideways by a (lateral) piezo and can deflect laterally. The upper calcite crystal slides at constant velocity V in reciprocating motion (12 µm in each direction), while it rubs the bottom crystal (V = 0) under an applied load L. The cantilever deflection in the lateral direction is used to determine the lateral force F_L , while the normal deflection of the bottom cantilever gives the normal load; $k_N=1000$ N/m and $k_L=256$ N/m are the spring constants in normal and lateral direction, respectively. The load applied ranged from 1 to 3 mN. Over the duration of one experiment, the change in thickness ΔT is at most 50 nm, which leads to a change of the load of less than 0.05 mN, i.e. to a negligible change of load. Therefore, the load was not adjusted during the experiment. Note that the change in crystal thickness ΔT is perpendicular to the lateral deflection, and hence, it does not affect the lateral force measurement. The crystals were visualized by Scanning Electron Microscope (SEM) at the end of each experiment to determine the apparent contact area, which ranged between 348 and 2163 µm² across experiments. The average stress was determined with the applied load and the apparent contact area.

The change in crystal thickness and friction are measured simultaneously. Figure 1B shows representative measurements of ΔT with time under an applied load of 2 mN at three different sliding velocities. The crystal thickness changes in an oscillatory fashion synchronized with the lateral motion of the surface. This is because the interferometric measurement is performed on a

fixed spot along the optical path (diameter of $\sim 2~\mu m$), but the reciprocating motion of the upper crystal implies that the measurement of ΔT takes place at different locations on the upper crystal (along the white line in bottom inset, Figure 1A). The cleavage of calcite leads to the formation of a few terraces (Figure S2), which are responsible for the initial roughness; in the example shown in Figure 1B, the initial variation of crystal thickness is \pm 2.5 nm (roughness amplitude), but it increases to \pm 7.5 nm during the experiment due to local dissolution/precipitation. Roughening was also observed under static loading in our previous experiments [14]. If the motion stops (0 μ m/s, black dots in Figure 1B), the oscillation vanishes because ΔT is measured at a fixed position on both crystals (Figure 1A, red dot in bottom right inset). To exclude the effect of the roughness from the pressure solution rate (r) we fit following expression to the experimental results:

$$\Delta T = \Delta T_0 + r \cdot t + a \cdot \sin(2\pi V(t + t_0)/d)$$

Eq. 1

Where t is the time, a the roughness amplitude along the scan distance, d the scan distance (12 μ m in these experiments) and ΔT_0 the known change of the crystal thickness at point of time t_0 at which the velocity V is first applied. Figure 1E shows the pressure solution rate r determined as a function of velocity and load. A negative rate pressure solution rate r indicates dissolution and a positive rate indicates precipitation.

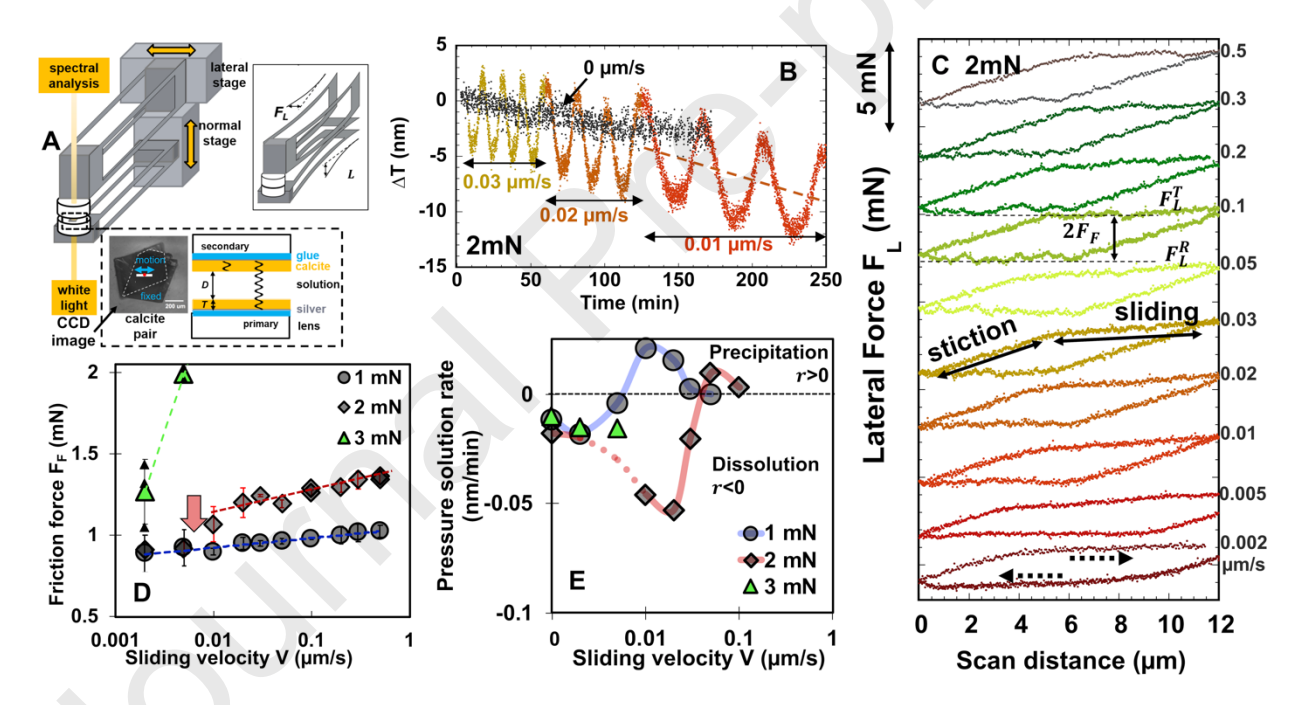


Figure 1. SFA results for pressure solution and friction between calcite single crystals in calcium carbonate (CaCO₃) saturated solution. **A** SFA schematics with lateral and normal springs, interferometer definition and an image of the two crystals in contact taken with a CCD camera during the measurement. **B** Change in crystal thickness under an applied load of 2 mN at 3 sliding velocities and under non sliding conditions (0 μm/s). The decrease in thickness, *i.e.*, Δ T<0, indicates dissolution. The oscillation is due to the variation of the crystal thickness along the sliding plane (roughness amplitude, *a*). The slope of the linear fit gives the pressure-induced dissolution rate. **C** Measured lateral force F_L as a function of total sliding distance at sliding velocities from 0.002 to 0.5 μm/s and an applied load of 2 mN. **D** Kinetic friction F_F vs. sliding velocity at normal loads of 1, 2 and 3 mN. The error bars give the variation in friction across 7 different friction loops at each speed. The red arrow in Figure 1D indicates the deviation of the friction force from the

logarithmic relation at low velocities under an applied load of 2mN. E Pressure-solution rate during the friction-force measurements; $0 \mu m/s$ indicates non-sliding. Initial crystal thickness = $19.544 \mu m$.

Figure 1C displays the lateral force F_L measured during the reciprocating motion of the crystal under a load of 2 mN and at sliding velocities between 2 nm/s and 0.5 µm/s; the piezo displacement at all velocities is 12 μ m (labelled as scan distance) in each direction. Each loop gives F_L while sliding to the right and left (see dashed arrows). The initial slope of the lateral force in each direction happens when the piezo moves and pulls the upper surface, but the two surfaces stick to each other so that there is no motion of the upper crystal, and the spring deflects ("stiction" period). When "sliding" starts, the kinetic friction force F_F is determined as the half of the loop width, F_F = $\frac{1}{2}(F_L^T - F_L^R)$. The average friction force from 7 cycles is shown in Figure 1D as a function of the sliding velocity and load. Under a load of 1 mN, friction changes logarithmically with the sliding velocity. Such a logarithmic trend is characteristic of a thermally activated shear assisted slip process [32] based on Eyring's transition state theory [33, 34]. Here, the jump frequency of the confined liquid molecules, ν , is increased by the shear stress τ according to $\nu \sim \nu^* \exp(-(E_a))$ $-\tau\phi$)/ k_BT), where E_a is the activation energy; ϕ a shear-activated volume, and ν^* a characteristic frequency of water and ions. The work imposed by the shear stress on each molecule $\tau\phi$ leads to a decrease of the energy barrier and facilitates slip. This yields following expression for the friction force $F_{\rm L}$ [32]:

$$F_{\rm L} = A \frac{E_a}{\phi} + A \frac{k_{\rm B}T}{\phi} \ln \left(V/V_0 \right)$$

Eq. 2

 $k_{\rm B}$ being the Boltzmann constant, T the absolute temperature, A the contact area and V_0 a reference velocity above which the thermal activation vanishes.

The dashed lines in Figure 1D show the fit of Eq. 2 to the experimental results at 1 and 2 mN. Note that this logarithmic relation was also observed when an oxidized silicon tip slid on the surface of a calcite crystal [21, 26]. Assuming A to be the apparent contact area, the fit of Eq. 2 to the experimental results yields a shear activation volume ϕ of 32.4 nm³. At an applied load of 2 mN, a decrease of friction below the logarithmic prediction (red dashed line) is observed at V < 0.02 µm/s (Figure 1D, red arrow). Hence, the fit to Eq. 2 is only possible at $V \ge 0.02$ µm/s with $\phi \sim 25.6$ nm³. ϕ has been interpreted as the size of the shear units, here composed of ions (Ca²⁺ and HCO₃-) and water, moving collectively in the thin fluid film separating the two surfaces during the sliding process. The smaller value of ϕ with load indicates the decreasing size of the shear units in the confined fluid film, perhaps resulting from the squeeze-out of ions and water with an increase in load. However, note that the contact area A has been assumed to be the apparent contact area, and hence, this only provides a rough estimation of ϕ , which must be considered with caution. Our previous work [21] evaluated in detail the variation of ϕ with load for silica-calcite interfaces at the level of a single asperity contact.

Figure 1E shows the concurrent pressure solution rate. Plastic deformation happens at applied stresses > 1 GPa [35], which is not the case here (<10 MPa), and the elastic deformation does not depend on the rate of deformation and thereby neither on velocity. Hence, the change in crystal thickness cannot be attributed to elastic or plastic deformation, but only to pressure solution. Importantly, the decrease of friction at V<0.02 μ m/s and 2 mN (Figure 1D, red arrow) is concurrent

with the maximum dissolution rate of calcite measured (r = -0.053 nm/min), while the dissolution rate at V > 0.03 µm/s is negligible. It is worthy of note that the change of friction force with velocity is reversible: the sliding velocity was first decreased, and a frictional weakening was observed; then, the friction force increased upon an increase in velocity to the original value (see the superposed data points at 0.1 and 0.5 µm/s in Figure 1D). This excludes that the evolution of the contact topography (e.g. due to roughening) is responsible for the observed frictional weakening.

Thermodynamics and kinetics justify that dissolution only happens at sufficiently slow sliding velocities and high loads. The increase in chemical potential $\Delta\mu$ with the normal stress drives the dissolution of the stressed calcite. This is because any applied pressure on the mineral increases its solubility $(a^p > a^0)$ and leads to a dramatic undersaturation of the interfacial solution, following $\Delta \mu/k_{\rm B}T = V_{\rm m}\sigma_{\rm n}/k_{\rm B}T = \ln(a^{\rm p}/a^{\rm 0})$, V_m being the molecular volume of calcite, and $a^{\rm 0}$ and $a^{\rm p}$ the activity of the solution in equilibrium with stress-free and stressed calcite, respectively[36]. For dissolution to happen, the contact time needs to be larger than the dissolution time. For instance, a pressure solution rate $r^p \sim -0.053$ nm/min implies the dissolution of $-r^p c^2/V_m \sim 0.216$ formula units of calcium carbonate per minute, where c^2 is the area of the unit cell of calcite (0.25 nm²). This means that one formula unit is dissolved in $\Delta t = 1/(r^p) \sim 278$ s at 2 mN ($\sigma_n \sim 5.74$ MPa). Taking the sliding length $d=12 \mu m$, it requires a velocity slower than $V_c = d/\Delta t = 0.043 \mu m s^{-1}$ for dissolution to happen at this stress. Theoretically, sliding events at either slower velocity (to allow longer contact times), or higher stress (to enhance the dissolution rate) should let calcite dissolution happen while sliding. This agrees well with the observation that $r^p < 0$ at $V \le 0.03$ μm/s. We thus propose that the pressure-induced dissolution of calcite leads to the presence of more ions in the confined fluid film, which re-hydrate and replenish the confined fluid film and thus provide more efficient lubrication. This phenomenon was previously observed at a single asperity contact between a calcite single crystal and a silicon tip and called "pressure-solution facilitated slip" [26]. Here, we demonstrate the relation between the pressure-induced dissolution of calcite and the frictional weakening of a macroscale calcite-calcite contact.

At a load of 1 mN (σ_n ~2.9 MPa), the pressure solution rates are smaller, and even positive, pointing toward precipitation within the contact (Figure 1E). Precipitation could happen either outside of the region measured by interferometry (white line in Figure 1A), causing a repulsion and separation of the two calcite crystals, which would be reflected in an increase of ΔT , or within the measuring region so that ΔT would include the thickness of the precipitate, as well. In either case, the occurrence of precipitation $(r^p > 0)$ requires that the confined fluid film between the two calcite crystals becomes supersaturated, at least locally. For growth to happen under an applied pressure σ_n , the supersaturation must fulfill $\tilde{\sigma} > \exp(\tilde{V}_m \sigma_n / RT)$ [37]. The crystal may also grow unstressed in groves and pits if $\tilde{\sigma} > 1$. Since the bulk solution is saturated with respect to calcite, the excess of ions in the confined fluid film may stem from the previous stress-induced dissolution of calcite, so that the dissolved mineral remains trapped in the confined fluid phase and leads to a local supersaturation. We have not investigated the nature of the precipitate but previous works have shown that amorphous calcium carbonate nanoparticles can grow under confinement between glass surfaces at low calcium carbonate concentrations [38]. SFA experiments on polycrystalline calcite films have also shown that an amorphous precipitate can form; the precipitate does not attach to the surfaces and a repulsive force acts between the calcite films, thereby hindering cementation [39]. In contrast, our results on calcite single crystals show that the kinetic friction slightly increases while sliding takes place with concurrent precipitation; Figure S5 illustrates this at two different sliding velocities. This suggests certain strengthening (cementation) of the contact during precipitation. Perhaps the use of calcite single crystals instead of rough polycrystalline films is the origin for the discrepancy between results, but more studies on rough surfaces are needed to

understand the more complex underlying mechanisms. Furthermore, such strengthening has not been observed at the level of a single asperity in AFM experiments (see Figure 2), and hence, it might be associated with the larger size and small roughness of the calcite-calcite contacts in the SFA experiments.

Finally, when the load was increased to 3 mN ($\sigma_{\rm n}$ ~ 8.6 MPa), friction increased further. Sliding was observed at 2 and 5 nm/s with concurrent dissolution with measured rates of -0.015 nm/min and -0.016 nm/min, respectively. At faster sliding velocities, the static friction was too high for sliding to happen. This is because the sliding distance is limited to $d=12~\mu \rm m$ in our instrument, and hence, a friction force greater than $k_Ld=2.4~mN$ is not measurable with the current setup.

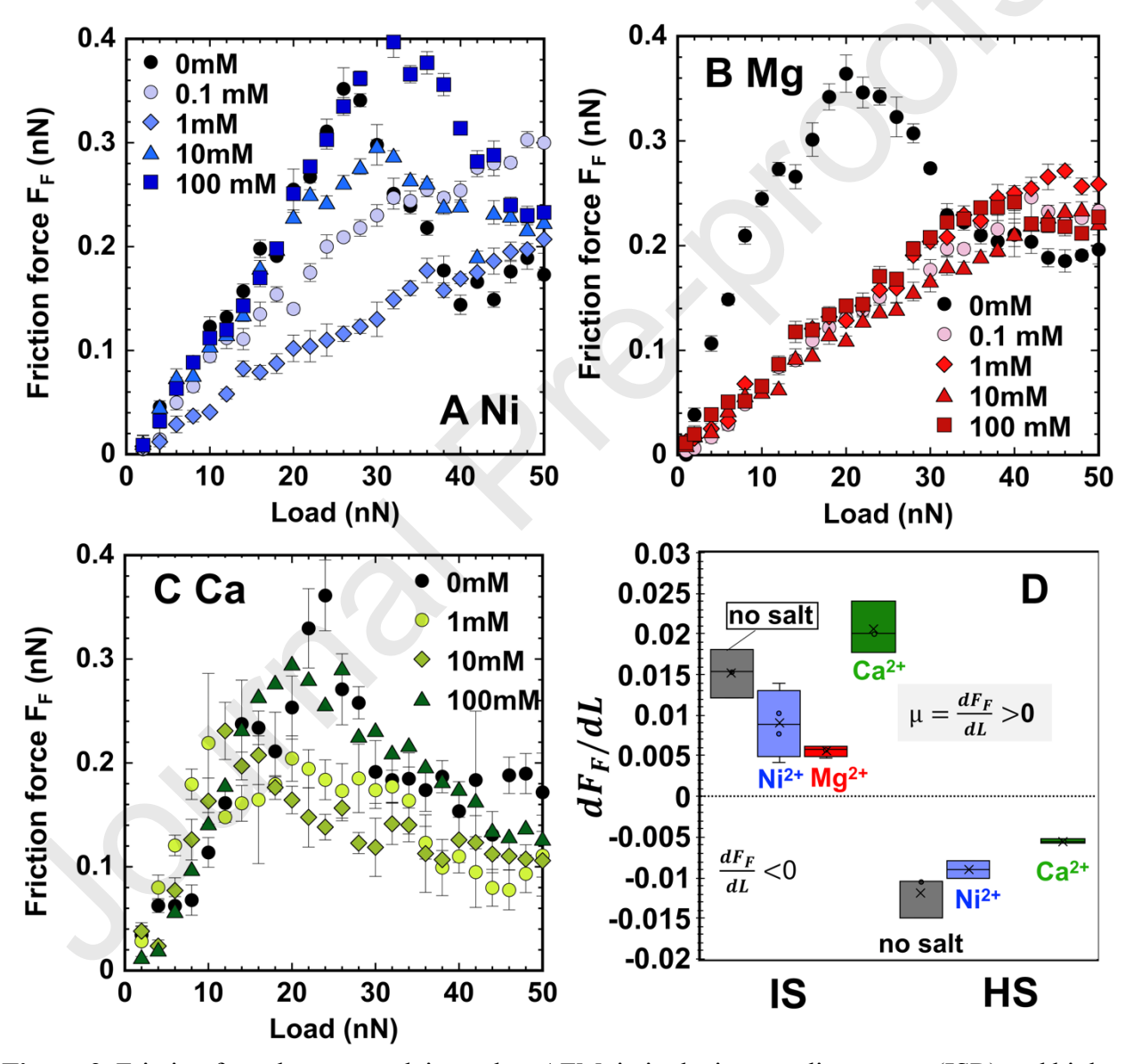


Figure 2. Friction force between calcite and an AFM tip in the intermediate-stress (ISR) and high-stress (HSR) regimes measured as a function of load in calcium carbonate saturated solution (0 mM, black), (A) NiCl₂, (B) MgCl₂ and (C) CaCl₂ solutions at a constant sliding velocity of 0.2 μm/s. An average friction is obtained from 8 friction loops per investigated condition and the error

bars show the standard deviation. The decrease in friction with increasing load reflects the pressure-solution facilitated slip. The color scheme is consistent throughout the work: blue for NiCl₂ solutions, red for MgCl₂ solutions and green for CaCl₂ solutions. The data for plot C were taken from Ref. [26], with open access license http://creativecommons.org/licenses/by/4.0/. (D) Friction coefficient (μ), calculated as the slope of the friction force vs. load ($\mu = \frac{dF_F}{dL} > 0$), representing the initial increase in friction with load. The initial slope of the decrease in friction with load ($\frac{dF_F}{dL} < 0$) is shown, as well.

3.2 Influence of fluid composition on friction

The effect of the fluid chemistry on friction was investigated by AFM at the level of a single asperity. Friction-force measurements were performed on the $(10\overline{1}4)$ cleavage plane of calcite single crystals with a (naturally oxidized) silicon tip at constant sliding velocity of 0.2 μ m/s. Calcite crystals were equilibrated in CaCO₃-saturated solutions for 24 h before adding NiCl₂, CaCl₂ or MgCl₂. Figure 2 shows representative results of the friction force as a function of normal load in solutions of NiCl₂, MgCl₂ and CaCl₂ at concentrations ranging from 0 mM to 100 mM. Note that the good reproducibility of results in different sets of experiments (i.e., different tips and calcite crystals) in equilibrium with water with 0 mM added salt (0.515 mM CaCO₃, labeled as "0 mM") ensures a quantitative comparison between experiments. In the three sets of experiments (black circles in Figures 2A-2C), friction increased with load (*L*) for *L*<20-25 nN, whereas a prominent decrease in friction with load was observed at higher loads.

The addition of salts led to a significant change of the friction force. The addition of MgCl₂ (Figure 2B) significantly reduced friction and eliminated the decreasing trend of friction with load at concentrations between 0.1 and 100 mM. CaCl₂ (Figure 2C) promoted pressure-solution facilitated slip, since the load above which friction decreased with increasing load was smaller than in the absence of added salt (0 mM, black). The addition of NiCl₂ (Figure 2A) led to an intermediate behavior. First, friction decreased by increasing the concentration to 0.1 and 1 mM, and no decrease in friction with an increase in load was detected. Increasing the concentration to 10 and 100 mM NiCl₂ led to an increase in friction while pressure-solution facilitated slip occurred above a load of ~ 30 nN. The quasi-lineal increasing friction with load gives the friction coefficient $\mu = d$ F_L/dL shown in Figure 2D and corresponding to the intermediate stress regime (ISR)[26]. The decreasing trend of friction with normal load reflects the pressure-solution facilitated slip. Because the tip cannot induce such a decrease in friction on a naturally oxidized silicon wafer or mica in aqueous solution, or on calcite in ethanol, where calcite is insoluble [21, 26], this must be associated with the pressure-induced dissolution of calcite. This happens when the load (stress) is high enough; we will refer to this range as high stress regime (HSR, see stress in Table S2). Figure 1D also shows the initial slope of F_L vs. L in the HSR $(dF_L/dL < 0)$.

3.3 Properties of the Confined Calcite/Solution Interface

To elucidate the origin of ion-specific and concentration-dependent effects on the friction force, the interfacial properties of calcite were investigated *via* surface force measurements by AFM. Force measurements were performed with both thermally annealed (oxidized) silicon tips and silica microspheres approaching the (1014) cleavage plane of a calcite single crystal at a velocity of 20 nm/s to avoid hydrodynamic effects; see details in SI text. Figure 3A-C shows representative force-separation curves as a function of the concentration of NiCl₂, MgCl₂ and CaCl₂ solutions, and in water equilibrated with calcium carbonate (0 mM). The exponentially decaying repulsive force dependent on ion concentration exhibits the characteristics of an electrical double layer force.

This indicates that the concentration of ions between the two surfaces is higher than in the bulk as a result of the attraction to the charged surfaces. The results show ion-specific and concentration-dependent effects on the surface forces.

The force has been normalized by the radius of the tip (R) to obtain a measure of the energy per unit area according to the Derjaguin approximation[40]. The Derjaguin-Landau-Verwey-Overbeek (DLVO) theory accounts for van der Waals and electrical double layer (EDL) forces between charged surfaces in aqueous solutions and it is used to evaluate the surface force at surface separations $D \gtrsim 5$ nm (i.e., long-range). Details about the model can be found in the SI Text. In brief, the Liftshitz theory was used to estimate the Hamaker constant (H=6.95 · 10⁻²¹ J for calcite vs. silica in aqueous solution). By solving the linearized Poisson-Boltzmann equation, an analytical expression for the EDL force is obtained, which is valid for dissimilar confining surfaces having low surface potentials (<25 mV) and mixtures of monovalent and multivalent ions. Low values for the zeta potential of calcite and silica have been reported in this concentration range[16], thereby justifying the linearization. The fits of the DLVO theory to the experimental results are shown in Figure 3A-C by the black lines and the diffuse potential of calcite, obtained as fitting parameter, is depicted in Figure 4A. The variability of the surface potential at 0 mM is due to the use of different calcite crystals in each experiment.

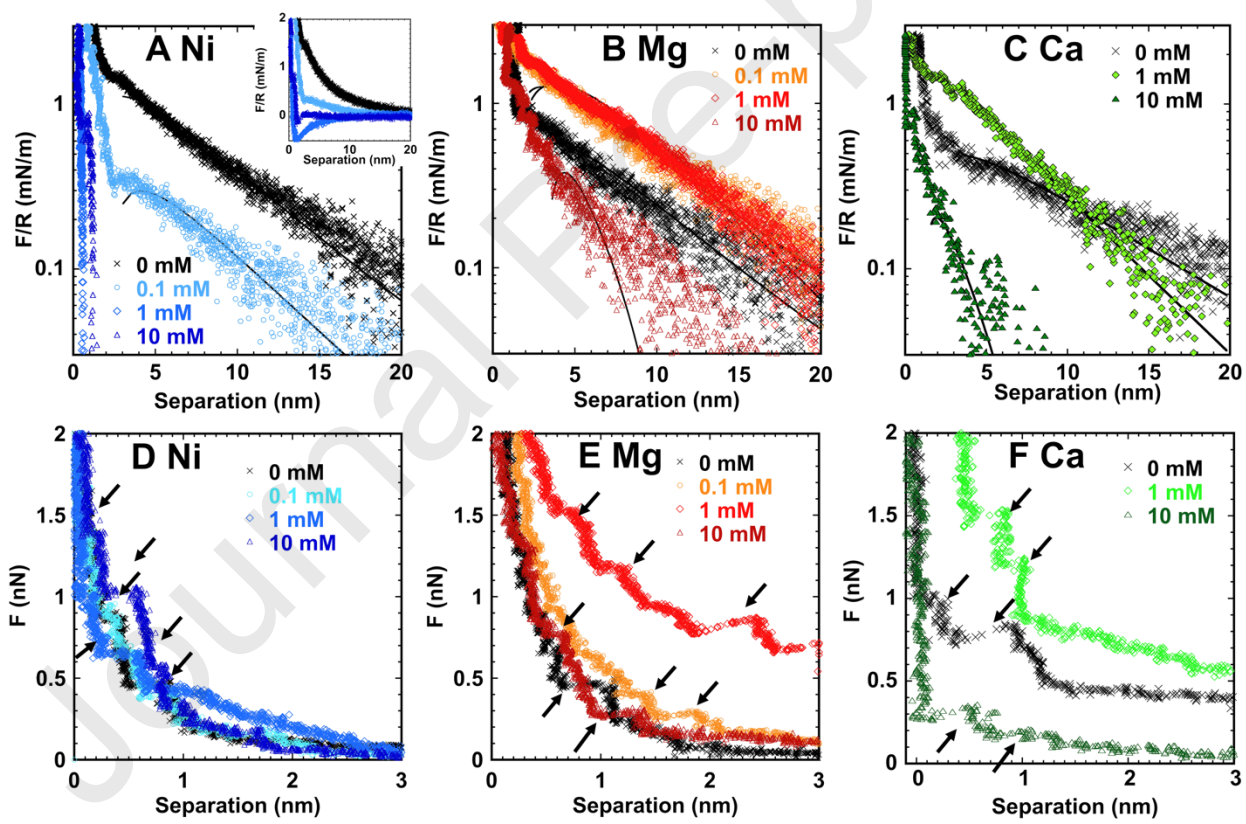


Figure 3. Representative surfaces forces between calcite single crystals and an AFM silica microsphere in (\mathbf{A}, \mathbf{D}) NiCl₂, (\mathbf{B}, \mathbf{E}) MgCl₂ and (\mathbf{C}, \mathbf{F}) CaCl₂ solutions. $(\mathbf{A}-\mathbf{C})$ Long-range surface force and fits of the DLVO theory to the experimental results; the diffuse potential of calcite is shown in Figure 4A. $(\mathbf{D}-\mathbf{F})$ Short-range (non-DLVO) force (D<3 nm). Steps (pointed by arrows) indicate the presence of interfacial layers.

The repulsive force detected at 0mM became less repulsive with an increase in NiCl₂ concentration

(Figure 3A). Because silicon oxide is negatively charged at the given pH of this experiment[41], a repulsive EDL force reflects the negative charge of the calcite surface, and hence, the counterions are the cations. The decay length of the repulsion decreased with increase in concentration and in good agreement with the Debye length of the solutions (7.7 nm and 7.2 nm, for 0 and 0.1 mM, respectively, Table S3). The diffuse potential of calcite became less negative in 0.1 mM NiCl₂ (from ~-10.9 to ~-6.6 mV, Figure 4A) and the surface charge became fully screened in ~ 1 mM NiCl₂, as inferred from the negligible electrical double layer force. The secondary minimum (see the negative force in the inset of Figure 3A) results from the superposed (attractive) van der Waals force. The less prominent minimum at 10 mM could stem from a charge reversal of both the calcite and silica surfaces, i.e. an overscreening of the surface charge by the absorbed Ni²⁺. In the case of CaCl₂ (Figure 3C), the EDL force became slightly stronger upon addition of 1 mM CaCl₂ to the saturated calcium carbonate solution (0 mM), while the diffuse potential decreased slightly (from -14.2 to -15.9 mV), indicating that, despite the increase in concentration, the counterions were not able to screen the surface charge. The collapse of the EDL force was prominent in 10 mM CaCl₂ (decay length=1.7 nm, Table S3) as expected from the Debye Hückel theory, and the diffuse potential of calcite dropped further to -3.9 mV. This behavior is qualitatively similar to that observed in NiCl₂, although a higher concentration of CaCl₂ is necessary to screen calcite's surface charge. These results are consistent with previously reported values for CaCl₂ [16].

The change of the EDL force with $MgCl_2$ concentration was in remarkable contrast (Figure 3B). First, the EDL repulsion became stronger with an increase in concentration to 0.1 and 1 mM, while a further increase to 10 mM led to a slight decrease in the repulsion. Interestingly, the diffuse potential clearly became more negative with $MgCl_2$ concentration (from -9.5 to -18.2 mV at 0 and 0.1 mM, respectively), which points towards an exchange of the counterions in the Stern layer, with Mg^{2+} being much less efficient in screening the surface charge. The increase of the EDL force at 1 mM $MgCl_2$ unambiguously reflects a more negative diffuse potential. However, the estimated diffuse potential is very high (-50.8 \pm 8.8 mV), and hence, this value might not be accurate. These results thus imply that both the affinity of Ni^{2+} to the calcite surface and its ability to screen surface charge are greater than for Ca^{2+} , and even more prominent compared to Mg^{2+} in the investigated range of concentrations.

The surface charge of calcite was roughly estimated using the Grahame equation. Because this equation is only rigorously valid for single surfaces, the results should be considered with caution. As shown in Table S4, the surface charge in the absence of added salt (0 mM) is ~-2 mC/m², and hence, it is one order of magnitude smaller than the reported surface charge of calcite based on X-ray reflectivity measurements of the adsorption of Rb+ (-20 mC/m²)[15]. Similar values (-1.3-6.0 mC/m²) are obtained in equilibrium with added salts, except for 1 mM MgCl₂ (-27.8 mC/m²). However, the diffuse potential is very high in this case, which makes the Debye Hückel approximation and this value invalid. While our results support the small surface charge of calcite in aqueous solution, the smaller values compared to ref. [15] might reflect certain charge regulation happening when the two surfaces approach each other [42], which does not occur on single surfaces.

The short-range (non-DLVO) surface force ($D \lesssim 3$ nm) exhibits steps or discontinuities (see arrows in Figure 3D-F). These steps are reminiscent of the oscillatory component of the hydration (non-DLVO) force between two smooth surfaces and it reflects that the water molecules and hydrated ions arrange in layers at the interface with the calcite surface [43, 44]. The steps happen when the AFM tip is approached toward the surface and jumps from one to the next layer.

3.4 Analysis of interfacial structure and energetics

The step size $\Delta = D_2 - D_1$ (D_2 and D_1 are the tip-calcite separation before and after the jump, as the tip approaches the surface) gives an estimate of the size of the molecules constituting this interfacial layer and is labeled as "layer thickness" in the following. A Gaussian distribution was fit to at least 200 steps per condition to determine the mean layer thickness and its frequency, which are shown in Figure 4B in a bubble chart as a function of salt concentration. The size of the bubble is proportional to the number of steps detected in the corresponding group, and hence, it represents the abundance of the layer. The classification of the interfacial structure is based on previous X-ray reflectivity measurements [45]: (i) $\Delta \sim 2-3$ Å is attributed to hydration layers (gray background in Fig. 4B); (ii) layers with $\Delta \sim 3-4$ Å are composed of ions of low hydration state, i.e. smaller hydration shell, so-called inner-sphere (IS) counterions; (iii) and layers with $\Delta \gtrsim 4$ Å are composed of more hydrated ions, so-called outer-sphere (OS) counterions. The force (F) required to probe these molecular layers with the tip reflects the strength of the interaction of water and ions with the calcite surface; molecules with stronger binding energy will require larger F values. Figures. 4C-E summarize the average force F as a function of layer thickness Δ . Note that the experiments were carried out with different tips, which affects the magnitude of the force. For example, the higher force in Figure 4E compared to Figures 4C-D arise from the use of a different tip. This is why we compare only results taken with the same tip in each plot.

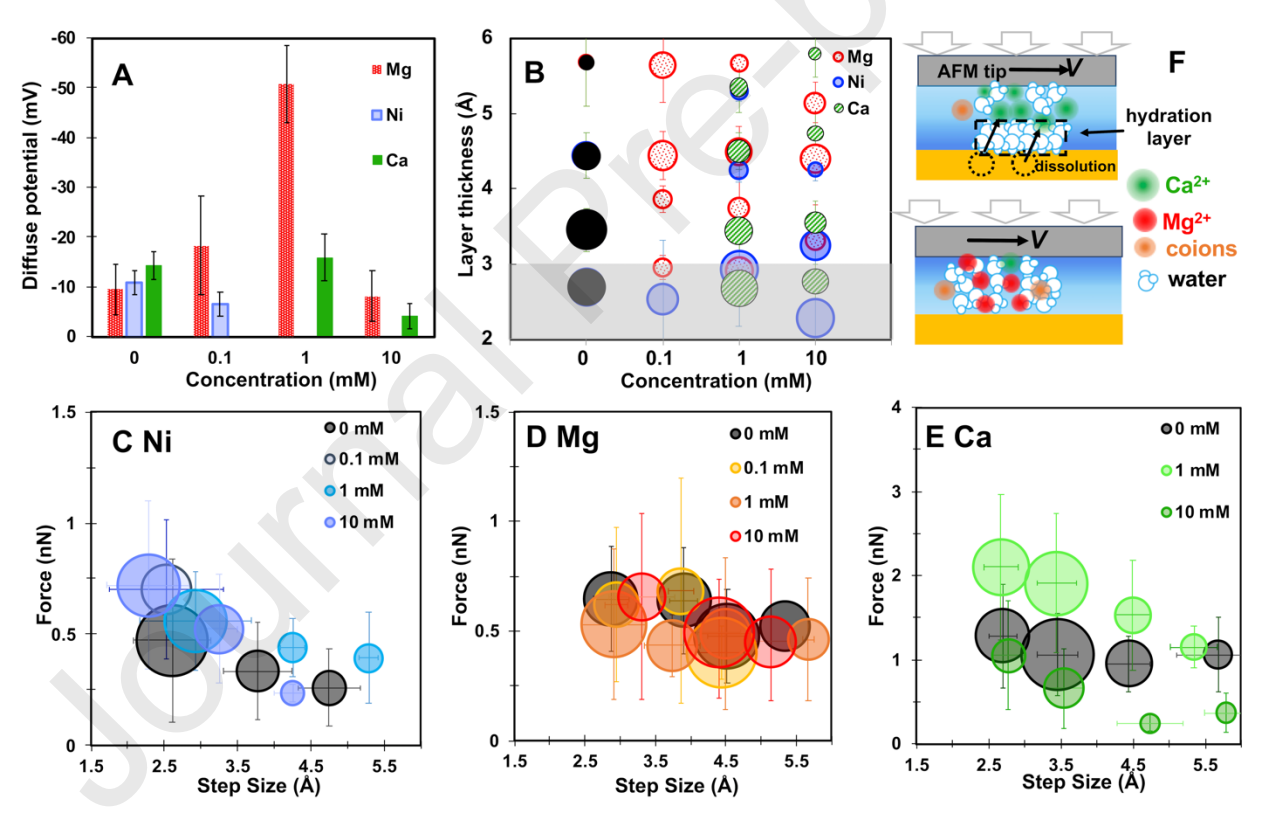


Figure 4. Diffuse potential and interfacial structure. (A) Diffuse potential of calcite in each solution. The variability of the surface potential at 0 mM (calcium carbonate saturated solution) is due to the use of different calcite single crystals in each experiment. At least 10 force curves are fit to obtain the diffuse potential per condition and the error bar is shown as the standard variation. The Debye length and the surface charge of silica are shown in Tables S3 and S5, respectively. (B) Bubble chart with the average thickness (Δ) of the resolved layers and the standard deviation (error bar), at least from 200 force curves per condition; gray background represents interfacial

layers closest to the calcite surface. The size of the bubble is proportional to the number of steps detected in the corresponding group, and hence, it represents the abundance or frequency of the layer. (C-E) Bubble diagram of the average force and the layer thickness obtained from the analysis of the hydration force in CaCO₃-saturated solution (0 mM, black), (C) NiCl₂, (D) MgCl₂ and (E) CaCl₂ solutions. (F) Conceptual picture of the confined fluid either with enrichment of Ca²⁺ or of Mg²⁺ ions during friction-force measurements.

In equilibrium with water (0 mM), calcite is negatively charged, and Ca²⁺ and hydronium are the counter-ions. In addition to the interfacial water layers (Δ ~2.7 Å in Figure 4B, black), layers with size Δ ~3.5 and 4.3 Å (likely IS-Ca²⁺) and a small number of layers with Δ ~5.7 Å (OS-Ca²⁺, see the small size of the bubble) are detected in this system [16]. The layer thickness with highest frequency (largest bubble in Figure 4B) is Δ ~2.7 Å, corresponding to interfacial water layers. The force applied to probe the interfacial structure decreases with an increasing Δ ; for instance, in Figure 4C, F~0.47, 0.33 and 0.26 nN for Δ ~2.7, 3.5 and 4.3 Å, respectively.

Upon the addition of 0.1 mM NiCl₂, only hydration layers with $\Delta \sim 2.53\pm0.78$ Å were detected, likely a mixture of water and IS-Ni²⁺, considering the large standard deviation. Ni exhibits the smallest hydration shell among the 3 cations (hydration shell diameter in the bulk, $d \sim 4.08$ Å) and highest hydration enthalpy. This, along with the results in Figure 4A, suggests a higher population of Ni²⁺ located closer to the surface than Ca²⁺ and screening the surface charge more efficiently, perhaps due to the smaller size of the hydrated complexes. In 1 mM NiCl₂ solutions, layers with OS-Ni²⁺ are detected (4.25 and 5.29 Å) but their frequency is still smaller than that of the interfacial water layers (2.93 ±0.76 Å); note that surface neutralization is already attained at this concentration. The layer closest to the surface exhibits a larger size compared to 0.1 mM, which suggests that more Ni²⁺ ions might accumulate closer to the surface and provide screening. In solutions with 10 mM NiCl₂, there is a drastic change of the interfacial structure; see the prominent decrease of the layer thickness probed closest to the surface to 2.28±0.56 Å and less OS-complexes. Force measurements at 10 mM support a charge reversal, as described earlier, and hence, it is possible that anions (HCO₃-, Cl⁻) are now present at the vicinity of the calcite surface.

The distribution of interfacial layers in $CaCl_2$ solutions reveals that hydration layers (2.67±0.23 and 2.77±0.23 Å at 1 and 10 mM, respectively) are located closest to the calcite surface, followed by the population of layers rich in IS-Ca²⁺ (3.43±0.27 and 3.54±0.29 Å) and OS-Ca²⁺ (>4.49 Å). Note that more layers are resolved for Ca^{2+} compared to Ni^{2+} , which is attributed to the more negative diffuse potential, and hence, to the lesser efficiency in screening the surface charge by Ca^{2+} compared to Ni^{2+} . The size of the hydration layers could suggest the presence of some IS- Ca^{2+} but the amount is smaller than for Ni^{2+} at the same concentrations, and hence, overall, Ca^{2+} is located further away from the surface. Note that the relation F vs. Δ follows a clear decreasing trend with increasing Δ at the investigated concentrations, like in the case of $NiCl_2$ (cf. Figure 4C and 4E). This reflects the thermodynamically structured solid/liquid interface under confinement, i.e., that more hydrated ions are located further away from the confined surface.

The size of the interfacial layers closest to the surface in MgCl₂ ($\Delta \sim 2.95\pm0.16$, and 2.91 ± 0.45 Å at 0.1, and 1 mM, respectively) also supports the presence of IS-Mg²⁺. However, the smaller bubble size compared to CaCl₂ and NiCl₂ indicates that Mg²⁺ significantly disturbs interfacial hydration layers. This has been proposed before based on molecular dynamic (MD) simulations (18). In addition, there is no clear relation between Δ and F; F lies in the range 0.37-0.68 mN/m (Figure 4D). All this suggests that the structure of the confined interface is significantly disturbed in MgCl₂ brines, in contrast to the results in water, NiCl₂ and CaCl₂ solutions. Although the origin for the

large magnitude of the negative diffuse potential (Figure 4A) is still unknown, the large value suggests that the surface-adsorbed IS-Mg²⁺ cannot screen the surface charge as efficiently as Ni²⁺ and Ca²⁺, and hence, it is consistent with the small size of the bubble corresponding to the layers located closest to the surface. Furthermore, this implies that more (mobile) Mg²⁺ counterions are needed further away from the surface to screen the diffuse potential, which justifies the much larger number of layers either rich in IS-Mg²⁺ (3.86±0.18, 3.74±0.4 and 3.31±0.47 Å), OS-Mg²⁺ (4.44±0.32, 4.49±0.34 and 4.40±0.30 Å), and more hydrated OS-Mg²⁺ (Δ -5.64±0.49, 5.67±0.08 and 5.14±0.27 Å), at 0.1, 1 and 10 mM, respectively, compared to the other brines. Table S6 in the SI summarizes the percentage of force curves that were measured over an area of 1 µm x 1 µm (a) with steps and (b) with steps larger than Δ ~3 Å, which represents layers of hydrated ions in the confined films. In fact, the latter is significantly higher for Mg²⁺ (>83%, except at 1mM) than for Ni²⁺ (<60%) and Ca²⁺ (<67%).

4. Discussion

Our measurements using the extended SFA provide a direct evidence for the relation between pressure-induced dissolution and frictional weakening of large contacts between calcite single crystals. This decrease in friction is also observed at nanoscale contacts between calcite and a naturally oxidized silicon tip as a result of calcite dissolution. The cartoon in Figure 4F (top) represents the proposed mechanism for pressure-solution facilitated slip. The surface-near concentration of counterions is much higher in the confined fluid film than the nominal brine concentration, which is due to the close proximity of the two (weakly) charged surfaces [40]. At the small pressures applied in SFA experiments (<10 MPa), multiple layers of ions and water remain confined between the two surfaces. At the high pressures of the AFM experiments (Table S2), only the most strongly adsorbed ions might remain in the contact. When the pressure solution is triggered, the contact is enriched with freshly dissolved calcium and carbonate ions. The confined fluid film thus becomes more lubricious with an increase in the population of dissolved and rehydrated ions. This is reminiscent of a phenomenon called hydration lubrication [46], which postulates that water molecules are retained between the confining surfaces forming part of the hydration shell of the ions, so they can maintain their high fluidity like in the bulk solution. This makes the confined films more lubricious than just pure water.

In addition to the pressure-solution facilitated slip, our SFA experiments show that the kinetic friction can also increase upon sliding due to the concurrent precipitation of calcite within the contact; a phenomenon that is not observed at single-asperity contacts in AFM experiments. The presence of a trapped fluid film in a larger contact thus enables precipitation within the contact (Figure 1D), which is associated with the strengthening (or cementation) of the contact and the increase in the friction coefficient.

Note that local variations in dissolution and precipitation are possible within large calcite-calcite contacts. This can lead to an increase in roughness over time, as shown in Figure 1B, and to a distribution of "true" contact pressures that, in turn, affects these local dissolution and precipitation processes. Such complexity is not captured in our measurements, since only a local (interferometric) measurement of the crystal thickness is possible. This is related to the friction force, which reflects the overall lubrication of the contact. Despite this, the relation proposed between the dissolution/precipitation rates and the friction force is evident, perhaps because such complexity is minimized on calcite single crystals with freshly cleaved surfaces. However, insight into how the influence of the local processes influences the friction force is still needed.

Previous studies of calcite-rich fault gouge have reported friction coefficients ~0.7 for dry contacts and ~0.6 under water saturated conditions [5]. We note that significantly lower friction coefficients are measured by AFM (0.005-0.025), while SFA experiments give values (0.3-0.4, Figure S6) comparable to fault gouge. There are multiple reasons for the discrepancy between the two methods. In the case of multi-asperity contacts, like in the SFA after roughening happens, asperity interlocking during sliding as well as asperity fracture and the described cementation can cause a significant increase in friction that is excluded in single asperity contacts [47-50], like in our AFM experiments. The relevance of ion-specific effects at the macroscale still needs to be investigated.

Our AFM measurements in the three salt solutions demonstrate that ion-specific and concentration-dependent mechanisms influence the friction between the tip and calcite (Figure 2), which we associate to the change of the interfacial composition. Ion-specific effects on solid/liquid interfacial properties are often attributed to the hydration characteristics of counter-ions: here, Ca²⁺ has a smaller hydration enthalpy than Mg²⁺ and Ni²⁺ (1577 kJ/mol *vs.* 1921 kJ/mol and 2105 kJ/mol, respectively [51]), and the radius of their respective first hydration shell extends to 3.5, 2.5 and 2.04 Å, respectively, as obtained from molecular dynamics for Mg²⁺ and Ni²⁺ [17] and extended X-ray absorption fine structure spectroscopy and DFT for Ni²⁺ [52]. However, the proximity of a surface can prevent metal cations from having a complete hydration shell due to the competition between surface and the counter-ions for water [17]. The short-range (non-DLVO) forces indicate that interfacial water layers are not disturbed by IS-Ca and OS-Ca complexes in CaCl₂ solutions, in agreement with our previous work [16, 21]. This is consistent with the visualization of the calcite-solution interface by AFM (Ricci et al., 2013), displaying the strongly hydrated calcium ions staying on top of calcite's hydration layers, also under the applied pressure with an AFM tip.

The decrease of the friction coefficient mediated by $MgCl_2$ is prominent and in remarkable contrast to the results for $CaCl_2$ (Figure 2D), while the corresponding interfacial structure is consistent with the distortion of the interfacial water layers. MD simulations (18) have showed that Mg^{2+} is able to bind water molecules from the surface to retain a full hydration shell. The stronger attraction of Mg^{2+} to the surface and the disruption of the interfacial water layers should favor the formation of an IS-Mg complex (size ~ 3.2 Å). Nevertheless, the large diffuse potential suggests that few counterions adsorb to calcite and screen the surface charge. This yield multiple layers of counterions close to the calcite surface (Figure 4B) and the presence of the hydrated ions decreases friction and favors hydration lubrication, in the same fashion as described earlier. Interestingly, the decrease in friction with an increase in load is not clearly observed in $MgCl_2$ solutions, which leads us to speculate about the need of interfacial water layers for pressure-solution facilitated slip to happen (Figure 4F). Note that the friction force at 0mM drastically decreases when the load exceeds ~ 20 nN and becomes smaller than that in $MgCl_2$ at the same load. It is possible that the interfacial structure after pressure-solution is more lubricious than the (hydrated) Mg^{2+} ions. However, this is speculative at this point and it requires further investigation.

The results for NiCl₂ are intriguing. Ni²⁺ has the highest hydration energy, and hence, a surface-induced dehydration of these cations is not likely. Ni²⁺, because of its smaller size and higher charge density could be more strongly bound to the negatively charged surface, and hence, a distortion of the interfacial water layers by Ni²⁺ could be possible; perhaps a distinction between water and IS-Ni is not possible due to their similar size. Note that this could happen at concentrations of 0.1 and 1 mM NiCl₂, while friction notably decreases, in a similar fashion as in MgCl₂ solutions. However, upon charge reversal at the concentration of 10 mM, friction increases, pressure solution facilitated slip is observed, and the interfacial structure undergoes also a

prominent change (Figure 4b). We hypothesize that this is related to the inclusion of Ni into calcite, which leads to a different population of counter-, co-ions and more water close to the calcite's surface. Incorporation of Ni²⁺ into the calcite lattice is promoted at smaller concentrations compared to Mg²⁺[53], which is consistent with this hypothesis, since charge neutralization of the calcite surface was not observed in MgCl₂ solutions. DFT simulations also show that the surface becomes more hydrophilic upon incorporation of Ni²⁺ into the lattice, which supports the presence of hydration water layers at 10 mM NiCl₂ [53].

We note that the coverage of (single) calcium surfaces with Rb⁺[15], Ca²⁺[19], and other divalent cations [19] has been reported to be small. For example, modeling the X-ray reflectivity data led to only ~ 1 Rb⁺ per every 40 unit cells. The number of layers detected with the AFM tip in the examined calcite crystals suggests a higher surface coverage. We do believe that a quantitative comparison to the reported surface coverage of unconfined calcite is not possible because the AFM tip probes the structure of the confined film between tip and calcite (~3 nm thick), and such confinement can enhance the number of trapped ions. Furthermore, recent comprehensive simulations and surface X-ray diffraction measurements [20] have demonstrated that Mg²⁺ does not adsorb on the basal plane of calcite, neither on the first nor second hydration layer. The deviation of these results from those by Kerisit and Parker[17] is attributed to the deficiencies in the force field (29). Hence, it is possible that we have not interpreted our results correctly and Mg²⁺ does not disturb the hydration layers. However, caution is needed when comparing our results to the behavior of the unconfined calcite/solution interface, because the confinement provided by the tip and the applied pressure have a deniable influence on the properties of the confined fluid, and therefore, we believe that differences between the unconfined and confined calcite/solution interface are possible.

While our picture for the interfacial structure appears to explain well friction and the onset of pressure solution facilitated slip, it is also well-known that the dissolution rate of calcite is affected by the pH of the solution [54]. In particular, a decrease of the dissolution rate of calcite has been reported above a pH of ~8 [55] and with an increase in pH from 7 to 9 [56]. This might be because the dissolution of calcite is mediated by hydronium ions, which simultaneously hydrolyze calciumcarbonate bonds and rapidly transfer a proton to fully hydrate calcite [55]. Table S1 shows the pH of the investigated solutions equilibrated with calcite, both measured prior to the AFM experiments and calculated by MINTEQ. There is a slight decrease in pH with an increase in concentration in CaCl₂ and NiCl₂ brines (from 8.35 to 7.54 and from 8.18 to 7.90, respectively), which is consistent with the promoted pressure solution in CaCl₂ brines and at high NiCl₂ concentrations; while MgCl₂ brines have the highest pH values (from 8.18 to 8.39). We do not know the pH and speciation in the confined fluid film that mediate the pressure solution of calcite under the tip. However, we cannot exclude that they are related to the bulk pH and speciation, and affect the solubility of the stressed calcite, thereby contributing to the pressure solution rate, as well. Similarly, the incorporation of metal cations into the crystal lattice could affect the pressure solution of calcite; this is currently under investigation.

5. Conclusion

This work directly studies the relation between pressure solution of calcite and the frictional strength of calcite-calcite contacts using an extended SFA with calcite single crystals for the first time. Note that previous studies had hypothesized a relation between pressure solution of calcite and friction based on AFM friction measurements [21, 26]. However, the SFA experiments

presented here not only provide the first direct evidence of this relation, but also expand further the current knowledge. Previous studies by SFA have shown the pressure-induced dissolution of polycrystalline calcite films[57] and freshly cleaved calcite single crystals [14], the resulting roughening of the contact and a repulsion acting between the surfaces, related to calcite hydration, roughness [57] and/or precipitation [39]. The present work reveals both weakening and strengthening of the frictional strength of the contact between calcite single crystals due to pressure solution in calcium-carbonate saturated water. In addition, our AFM experiments show that the friction coefficient of calcite at the level of a single-asperity contact is strongly dependent on the interfacial composition. While previous studies had investigated the effects of NaCl and CaCl₂, the influence of three divalent cations has been compared here, which has revealed new underlying mechanisms. As previously reported, interfacial water layers of calcite remain undisturbed in the presence of Ca(II), where pressure solution is enhanced and the dissolved ions lubricate the surface to reduce the friction coefficient. In contrast, Mg(II) and low concentrations of Ni(II) disrupt the ice-like hydration structure of the calcite surface forming more fluid-like layers, which cause a prominent decrease in the friction coefficient. Pressure-solution facilitated slip is also promoted through the neutralization of the charge of the calcite surface (e.g. at high Ni(II) concentration) due to the modification of calcite's hydration layers.

Down to several km depth in the subsurface, nanometer thin water films are also maintained between contacting mineral surfaces while they sustain the overburden pressure. Although the investigated systems by SFA and AFM are oversimplified compared to rock interfaces at faults, this simplification facilitates the understanding of microscopic mechanisms that can be extrapolated to geological scales. Most induced seismicity in the Midwestern US has been attributed to the disposal of large volumes of coproduced wastewater from oil and gas extraction [58], which are brines of high salinity. The effect of water on seismic activities is generally attributed to a reduction in effective normal stress, hydrothermal alteration, and precipitation of different minerals at fault planes [22, 59]. The nanoscale insight provided by our experiments demonstrates that pressure solution can not only cause cementation but also lead to a significant weakening of the fault strength of single-asperity contacts. Our findings also call for a reassessment of the treatment of coproduced water before injection, since the frictional weakening strongly depends on the fluid composition. The complexity of the natural interfaces, with pits and grooves, could lead to additional contributions to the fault strength, such as interlocking asperities between rough surfaces and the increase in true contact area due to pressure solution, which we have not considered yet. Ongoing studies of the effect of calcite's roughness on the friction coefficient will further help extrapolate our results to macroscale fault dynamics.

CRediT authorship contribution statement

Binxin Fu: Methodology, Investigation, Formal Analysis, Visualization, Writing – original draft. **Yijue Diao:** Methodology, Formal Analysis, Investigation.

Rosa M. Espinosa-Marzal: Conceptualization, Formal Analysis, Supervision, Visualization, Writing – review & editing, Funding acquisition.

Declaration of competing interest

The authors declare that they have no known competing financial interests or personal relationships that could have appeared to influence the work reported in this paper.

Acknowledgements

This work was supported by the National Science Foundation under grant No. NSF EAR 18-56525

and research board of University of Illinois Urbana-Champaign (UIUC). We also would like to give deep gratitude to Prof. Manfred Heuberger for fruitful discussions about the extension of the SFA. Calcite sample preparation for SFA experiments were carried out in the Materials Research Laboratory Central Research Facilities, University of Illinois at Urbana-Champaign.

References

- [1] J.-P. Gratier, D.K. Dysthe, F. Renard, The Role of Pressure Solution Creep in the Ductility of the Earth's Upper Crust, in: R. Dmowska (Ed.), Adv. Geophys., Elsevier 2013, pp. 47-179.
- [2] E. Gundersen, F. Renard, D.K. Dysthe, K. Bjorlykke, B. Jamtveit, Coupling between pressure solution creep and diffusive mass transport in porous rocks, J. Geophys. Res. Solid Earth 107 (2002).
- [3] F.M. Chester, N.G. Higgs, Multimechanism Friction Constitutive Model for Ultrafine Quartz Gouge at Hypocentral Conditions, J. Geophys. Res. Solid Earth 97 (1992) 1859-1870.
- [4] P.K. Weyl, Pressure Solution and the Force of Crystallization a Phenomenological Theory, J. Geophys. Res. 64 (1959) 2001-2025.
- [5] B.A. Verberne, C.J. Spiers, A.R. Niemeijer, J.H.P. De Bresser, D.A.M. De Winter, O. Plümper, Frictional Properties and Microstructure of Calcite-Rich Fault Gouges Sheared at Sub-Seismic Sliding Velocities, Pure and Applied Geophysics 171 (2014) 2617-2640.
- [6] B.M. Carpenter, C. Collettini, C. Viti, A. Cavallo, The influence of normal stress and sliding velocity on the frictional behaviour of calcite at room temperature: insights from laboratory experiments and microstructural observations, Geophys. J. Int. 205 (2016) 548-561.
- [7] M.M. Scuderi, C. Collettini, C. Marone, Frictional stability and earthquake triggering during fluid pressure stimulation of an experimental fault, Earth Planet. Sci. Lett. 477 (2017) 84-96.
- [8] S. Zubtsov, F. Renard, J.-P. Gratier, D.K. Dysthe, V. Traskine, Single-contact pressure solution creep on calcite monocrystals, Deformation Mechanisms, Rheology and Tectonics: From Minerals to the Lithosphere 243 (2005) 81-95.
- [9] D. Croizé, F. Renard, K. Bjørlykke, D.K. Dysthe, Experimental calcite dissolution under stress: Evolution of grain contact microstructure during pressure solution creep, J. Geophys. Res. 115 (2010).
- [10] X. Zhang, C.J. Spiers, Compaction of granular calcite by pressure solution at room temperature and effects of pore fluid chemistry, Int. J. Rock. Mech. Min. 42 (2005) 950-960.
- [11] X. Zhang, C.J. Spiers, Effects of phosphate ions on intergranular pressure solution in calcite: An experimental study, Geochimica et Cosmochimica Acta 69 (2005) 5681-5691.
- [12] E. Liteanu, C.J. Spiers, Influence of pore fluid salt content on compaction creep of calcite aggregates in the presence of supercritical CO2, Chemical Geology 265 (2009) 134-147.
- [13] J. Wheeler, Anisotropic rheology during grain boundary diffusion creep and its relation to grain rotation, grain boundary sliding and superplasticity, Philosophical Magazine 90 (2010) 2841-2864.
- [14] Y.J. Diao, A.Q. Li, R.M. Espinosa-Marzal, Ion specific effects on the pressure solution of calcite single crystals, Geochimica et Cosmochimica Acta 280 (2020) 116-129.
- [15] S.S. Lee, F. Heberling, N.C. Sturchio, P.J. Eng, P. Fenter, Surface Charge of the Calcite (104) Terrace Measured by Rb+ Adsorption in Aqueous Solutions Using Resonant Anomalous X-ray Reflectivity, J. Phys. Chem. C 120 (2016) 15216-15223.
- [16] Y. Diao, R.M. Espinosa-Marzal, Molecular insight into the nanoconfined calcite-solution interface, Proc. Natl. Acad. Sci. U S A 113 (2016) 12047-12052.
- [17] S. Kerisit, S.C. Parker, Free energy of adsorption of water and metal ions on the [1014] calcite surface, J. Am. Chem. Soc. 126 (2004) 10152-61.
- [18] M. Ricci, P. Spijker, F. Stellacci, J.F. Molinari, K. Voitchovsky, Direct visualization of single ions in the Stern layer of calcite, Langmuir 29 (2013) 2207-16.
- [19] P. Raiteri, J.D. Gale, D. Quigley, P.M. Rodger, Derivation of an Accurate Force-Field for Simulating the Growth of Calcium Carbonate from Aqueous Solution: A New Model for the

- Calcite-Water Interface, J. Phys. Chem. C 114 (2010) 5997-6010.
- [20] S.J.T. Brugman, P. Raiteri, P. Accordini, F. Megens, J.D. Gale, E. Vlieg, Calcite (104) Surface-Electrolyte Structure: A 3D Comparison of Surface X-ray Diffraction and Simulations, J. Phys. Chem. C 124 (2020) 18564-18575.
- [21] Y. Diao, R.M. Espinosa Marzal, Effect of Fluid Chemistry on the Interfacial Composition, Adhesion, and Frictional Response of Calcite Single Crystals—Implications for Injection Induced Seismicity, J. Geophys. Res. Solid Earth 124 (2019) 5607-5628.
- [22] C. Meller, T. Kohl, The significance of hydrothermal alteration zones for the mechanical behavior of a geothermal reservoir, Geotherm. Energy 2 (2014) 12.
- [23] J. Heinicke, T. Fischer, R. Gaupp, J. Gotze, U. Koch, H. Konietzky, K.P. Stanek, Hydrothermal alteration as a trigger mechanism for earthquake swarms: the Vogtland/NW Bohemia region as a case study, Geophys. J. Int. 178 (2009) 1-13.
- [24] V. Vavryčuk, P. Hrubcová, Seismological evidence of fault weakening due to erosion by fluids from observations of intraplate earthquake swarms, J. Geophys. Res. Solid Earth 122 (2017) 3701-3718.
- [25] P. Baker, M. Kastner, J. Byerlee, D. Lockner, Pressure solution and hydrothermal recrystallization of carbonate sediments—an experimental study, Mar. Geol. 38 (1980) 185-203.
- [26] Y. Diao, R.M. Espinosa-Marzal, The role of water in fault lubrication, Nature Communications 9 (2018) 2309.
- [27] C.-Y. Yang, Calcium and magnesium in drinking water and risk of death from cerebrovascular disease, Stroke 29 (1998) 411-414.
- [28] L.A. Hardie, Origin of CaCl 2 brines by basalt-seawater interaction: Insights provided by some simple mass balance calculations, Contrib. Mineral. Petrl. 82 (1983) 205-213.
- [29] L.Z. Lakshtanov, S.L.S. Stipp, Experimental study of nickel(II) interaction with calcite: Adsorption and coprecipitation, Geochimica et Cosmochimica Acta 71 (2007) 3686-3697.
- [30] Y.-P. Lin, P.C. Singer, Effect of Mg2+ on the kinetics of calcite crystal growth, J. Cryst. Growth 312 (2009) 136-140.
- [31] M. Heuberger, The extended surface forces apparatus. Part I. Fast spectral correlation interferometry, Review of Scientific Instruments 72 (2001) 1700-1707.
- [32] B.J. Briscoe, D.C.B. Evans, The shear properties of Langmuir—Blodgett layers, Proc. R. Soc. A 380 (1997) 389-407.
- [33] H. Eyring, The activated complex in chemical reactions, The Journal of Chemical Physics 3 (1935) 107-115.
- [34] H. Eyring, Viscosity, plasticity, and diffusion as examples of absolute reaction rates, The Journal of Chemical Physics 4 (1936) 283-291.
- [35] J.H. Dieterich, B.D. Kilgore, Imaging surface contacts: power law contact distributions and contact stresses in quartz, calcite, glass and acrylic plastic, Tectonophysics 256 (1996) 219-239.
- [36] J. Schott, S. Brantley, D. Crerar, C. Guy, M. Borcsik, C. Willaime, Dissolution kinetics of strained calcite, Geochimica et Cosmochimica Acta 53 (1989) 373-382.
- [37] M. Steiger, Crystal growth in porous materials I: The crystallization pressure of large crystals, J. Cryst. Growth 282 (2005) 455-469.
- [38] Y.W. Wang, M.L. Zeng, F.C. Meldrum, H.K. Christenson, Using Confinement To Study the Crystallization Pathway of Calcium Carbonate, Crystal Growth & Design 17 (2017) 6787-6792.
- [39] J. Dziadkowiec, B. Zareeipolgardani, D.K. Dysthe, A. Royne, Nucleation in confinement generates long-range repulsion between rough calcite surfaces, Sci. Rep. 9 (2019) 8948.
- [40] J.N. Israelachvili, Intermolecular and Surface Forces, 3rd Edition, Elsevier, Amsterdam2011.
- [41] R.K. Iler, The chemistry of silica, Wiley, New York, 1979.
- [42] G. Trefalt, F.J.M. Ruiz-Cabello, M. Borkovec, Interaction Forces, Heteroaggregation, and Deposition Involving Charged Colloidal Particles, J. Phys. Chem. B 118 (2014) 6346-6355.
- [43] J.N. Israelachvili, R.M. Pashley, Molecular Layering of Water at Surfaces and Origin of Repulsive Hydration Forces, Nature 306 (1983) 249-250.
- [44] R.M. Espinosa-Marzal, T. Drobek, T. Balmer, M.P. Heuberger, Hydrated-ion ordering in electrical double layers, Phys. Chem. Chem. Phys. 14 (2012) 6085-93.
- [45] P. Fenter, S. Kerisit, P. Raiteri, J.D. Gale, Is the Calcite–Water Interface Understood? Direct

- Comparisons of Molecular Dynamics Simulations with Specular X-ray Reflectivity Data, The Journal of Physical Chemistry C 117 (2013) 5028-5042.
- [46] L. Ma, A. Gaisinskaya-Kipnis, N. Kampf, J. Klein, Origins of hydration lubrication, Nature Communications 6 (2015) 6060.
- [47] F.M. Chester, Effects of Temperature on Friction Constitutive-Equations and Experiments with Quartz Gouge, J. Geophys. Res. Solid Earth 99 (1994) 7247-7261.
- [48] H.M. Horn, D.U. Deere, Frictional Characteristics of Minerals, Géotechnique 12 (1962) 319-335.
- [49] B.C. Donose, I.U. Vakarelski, E. Taran, H. Shinto, K. Higashitani, Specific effects of divalent cation nitrates on the nanotribology of silica surfaces, Ind. Eng. Chem. Res. 45 (2006) 7035-7041.
- [50] E. Liu, B. Blanpain, J.P. Celis, J.R. Roos, Comparative study between macrotribology and nanotribology, Journal of Applied Physics 84 (1998) 4859-4865.
- [51] D.W. Smith, Ionic hydration enthalpies, J. Chem. Educ. 54 (1977) 540.
- [52] H.Y. Liu, C.H. Fang, Y. Fang, Y.Q. Zhou, H.W. Ge, F.Y. Zhu, P.C. Sun, J.T. Miao, Characterizing Ni(II) hydration in aqueous solution using DFT and EXAFS, J. Mol. Model. 22 (2016) 2.
- [53] M.P. Andersson, K. Dideriksen, H. Sakuma, S.L. Stipp, Modelling how incorporation of divalent cations affects calcite wettability-implications for biomineralisation and oil recovery, Sci. Rep. 6 (2016) 28854.
- [54] E.L. Sjöberg, D.T. Rickard, Calcite dissolution kinetics: Surface speciation and the origin of the variable pH dependence, Chemical Geology 42 (1984) 119-136.
- [55] R. Shiraki, P.A. Rock, W.H. Casey, Dissolution kinetics of calcite in 0.1 m NaCl solution at room temperature: An atomic force microscopic (AFM) study, Aquat. Geochem. 6 (2000) 87-108. [56] I.V. Dolgaleva, I.G. Gorichev, A.D. Izotov, V.M. Stepanov, Modeling of the effect of pH on the calcite dissolution kinetics, Theor. Found. Chem. Eng. 39 (2005) 614-621.
- [57] J. Dziadkowiec, S. Javadi, J.E. Bratvold, O. Nilsen, A. Royne, Surface Forces Apparatus Measurements of Interactions between Rough and Reactive Calcite Surfaces, Langmuir 34 (2018) 7248-7263.
- [58] W.L. Ellsworth, Injection-induced earthquakes, Science 341 (2013) 1225942.
- [59] J.H. Healy, W.W. Rubey, D.T. Griggs, C.B. Raleigh, The Denver Earthquakes, Science 161 (1968) 1301-10.

CRediT authorship contribution statement

Binxin Fu: Methodology, Investigation, Formal Analysis, Visualization, Writing – original draft. **Yijue Diao:** Methodology, Formal Analysis, Investigation.

Rosa M. Espinosa-Marzal: Conceptualization, Formal Analysis, Supervision, Visualization, Writing – review & editing, Funding acquisition.

Journal Pre-proofs

n	ഹി	laration	of interests
IJ	ec.	iaration	or interests

☐ The authors declare that they have no known comprelationships that could have appeared to influence the work					
☐The authors declare the following financial interests/personal relationships which may be considered as potential competing interests:					